Lateral inhomogeneity of the Mg/(Zn+Mg) composition at the (Zn,Mg)O/CuIn(S,Se)$_2$ thin-film solar cell interface revealed by photoemission electron microscopy

Bär, M.; Theisen, J. P.; Wilks, R. G.; Erfurth, F.; Félix, R.; Gerlach, D.; Haas, S.; Tati Bismaths, L.; Reinert, F.; Kronast, F.

Published in:
Journal of Applied Physics

DOI:
10.1063/1.4804413

Publication date:
2013

Journal of Applied Physics

Lateral inhomogeneity of the Mg/(Zn+Mg) composition at the (Zn,Mg)O/CuIn(S,Se)$_2$ thin-film solar cell interface revealed by photoemission electron microscopy

Cite as: J. Appl. Phys. **113**, 193709 (2013); https://doi.org/10.1063/1.4804413
Submitted: 28 March 2013 . Accepted: 25 April 2013 . Published Online: 20 May 2013

M. Bär, J.-P. Theisen, R. G. Wilks, F. Erfurth, R. Félix, D. Gerlach, S. Haas, L. Tati Bismaths, F. Reinert, F. Kronast, T. P. Niesen, J. Palm, S. Visbeck, and L. Weinhardt

AIP Publishing

Lateral inhomogeneity of the Mg/(Zn+Mg) composition at the (Zn,Mg)O/CuIn(S,Se)$_2$ thin-film solar cell interface revealed by photoemission electron microscopy

M. Bär,[1,2] J.-P. Theisen,[3] R. G. Wilks,[1] F. Erfurth,[3] R. Félix,[1] D. Gerlach,[1] S. Haas,[4] L. Tati Bismaths,[5] F. Reinert,[3,6] F. Kronast,[5] T. P. Niesen,[7] J. Palm,[7] S. Visbeck,[7] and L. Weinhardt[3,8,9]

[1]*Solar Energy Research, Helmholtz Zentrum Berlin für Materialien und Energie GmbH, Hahn-Meitner-Platz 1, D-14109 Berlin, Germany*
[2]*Institut für Physik und Chemie, Brandenburgische Technische Universität Cottbus, Konrad-Wachsmann-Allee 1, D-03046 Cottbus, Germany*
[3]*Universität Würzburg, Experimentelle Physik VII, Am Hubland, D-97074 Würzburg, Germany*
[4]*Functional Materials, Helmholtz Zentrum Berlin für Materialien und Energie GmbH, Hahn-Meitner-Platz 1, D-14109 Berlin, Germany*
[5]*Department for Magnetisation Dynamics, Helmholtz-Zentrum Berlin für Materialien und Energie GmbH, Albert-Einstein-Str. 15, D-12489 Berlin, Germany*
[6]*Gemeinschaftslabor für Nanoanalytik, Karlsruhe Institute of Technology, D-76021 Karlsruhe, Germany*
[7]*AVANCIS GmbH & Co. KG, Otto-Hahn-Ring 6, D-81739 München, Germany*
[8]*Institute for Photon Science and Synchrotron Radiation, Karlsruhe Institute of Technology, Hermann-v.-Helmholtz-Platz 1, D-76344 Eggenstein-Leopoldshafen, Germany*
[9]*ANKA Synchrotron Radiation Facility, Karlsruhe Institute of Technology, Hermann-von-Helmhotz-Platz 1, D-76344 Eggenstein-Leopoldshafen, Germany*

(Received 28 March 2013; accepted 25 April 2013; published online 20 May 2013)

Spatial variations in the chemical composition of the (Zn,Mg)O/CuIn(S,Se)$_2$ thin-film solar cell interface were studied by photoemission electron microscopy (PEEM). Energy filtered PEEM images indicate significant differences in the magnesium and zinc distribution. Local photoemission measurements reveal a relative difference in the derived Mg/(Zn+Mg) composition of the (Zn,Mg)O material of up to (11.4 ± 0.7)%, which can be expected to induce band gap fluctuations of (60 ± 30) meV. Furthermore, local areas with significant accumulations of sodium could be observed. © *2013 AIP Publishing LLC*. [http://dx.doi.org/10.1063/1.4804413]

INTRODUCTION

Thin-film solar cells based on the chalcopyrite absorber material system Cu(In$_{1-X}$Ga$_X$)(S$_Y$Se$_{1-Y}$)$_2$ (CIGSSe) represent one of the most promising technologies to compete with established Si-wafer based devices. High efficiencies, both for CIGSSe-based modules (9703 cm^2, 15.7%)[1] and for laboratory-scale solar cells (0.5 cm^2, 20.3%),[1,2] have already been demonstrated. For economical and ecological reasons, one of the main goals of today's research is the replacement of the standard CdS buffer layer (usually prepared by chemical bath deposition) in the n$^+$-ZnO/i-ZnO/buffer/CIGSSe/Mo/glass device structure. A very attractive alternative would be to sputter the n$^+$-ZnO/i-ZnO window bi-layer directly on the CIGSSe absorber. However, this approach leads to rather low cell efficiencies (see, e.g., Ref. 3). Minemoto *et al.* suggested replacing the i-ZnO with a (Zn,Mg)O layer.[4] Their study of the Mg/(Zn+Mg) composition dependence of the (Zn,Mg)O valence band (VB) position and the optical band gap led to the suggestion that the Mg-content can be used to tailor the conduction band alignment at the (Zn,Mg)O/CIGSSe interface. This was recently confirmed by Erfurth *et al.*, who directly measured the band alignment at the (Zn,Mg)O/absorber interface for several Mg/(Zn+Mg) ratios using a combination of direct and inverse photoemission.[5] Both studies show that best efficiencies are achieved when using a "suitable" Mg/(Zn+Mg) composition (17% in Ref. 4 and 29% in Ref. 5) that leads to a small spike-like conduction band offset.[4,5] For the absorber material used in our study, solar cell devices with a n$^+$-ZnO/Zn$_{0.7}$Mg$_{0.3}$O bi-layer directly sputtered on the chalcopyrite absorber resulted in efficiencies of up to 12.5%[6] (similar to those of corresponding CdS buffered reference cells: 13.2%).

In a previous study,[7] we investigated the formation of the (Zn,Mg)O/CuIn(S,Se)$_2$ (CISSe) interface by *spatially integrating* x-ray photoelectron spectroscopy (XPS), finding the incorporation of Zn in the uppermost region of the CISSe surface forming Zn-S or Zn-Se bonds. Furthermore, we discovered that as a result, the (Zn,Mg)O layer close to the (Zn,Mg)O/CISSe interface is Zn depleted (i.e., Mg-rich). Furthermore, recently we also studied the *spatially resolved* chemical and electronic surface structure of high-efficiency polycrystalline Cu(In,Ga)Se$_2$ absorbers by mapping the elemental distribution at the surface using photoemission electron microscopy (PEEM) revealing intergrain fluctuations.[8] In this letter we are using PEEM to *spatially resolve* the (Zn,Mg)O/CISSe interface structure. As result, we report on an interface structure which is rather complex not only *vertically* (as reported in Ref. 7) but also *laterally*.

EXPERIMENTAL

CIGSSe absorber layers were prepared onto Mo-coated glass in the Avancis pilot line (formerly Shell Solar, Munich)

by deposition of metal precursors and subsequent rapid thermal processing.[9] This results in CIGSSe films that are Ga-free (i.e., CISSe-like) at the surface.[10] (Zn,Mg)O buffer layers of 1 nm nominal thickness were deposited by rf-magnetron sputtering using the same sputter parameters as used for the samples investigated in our XPS study.[7] The MgO-content of the mixed (Zn,Mg)O target was 30%. The PEEM experiments were performed at the UE49-PGMa microfocus beamline (BESSY II synchrotron facility) using the SPEEM endstation equipped with an Elmitec PEEM II instrument[11] and ultraviolet (UV, Hg discharge lamp: 5.1 eV → Hg-PEEM) or soft x-ray excitation ($h\nu = 100$–1800 eV → X-PEEM). The PEEM images have been recorded with an accelerator voltage between sample and microscope lens of 10 keV and a field of view (FOV) of 10 μm. The images have been normalized to (i.e., divided by) a brightfield image recorded directly before the actual measurements to account for detector characteristics. In order to be able to correct for thermal drifts, a number of images (several 10 up to a few 100) have been recorded at relatively short measurement times (1–10 s). The final image was then computed by adding up the individual *drift-corrected* images.

Depending on the sample and the energy of the excitation, different mechanisms can generate a contrast in PEEM. When using excitation energies close above the work function of the sample, the electron emission intensity is dominated by the local work function of the sample. If excited with soft x-rays with an energy slightly above an absorption edge of an element present at the sample surface, the PEEM images become chemical sensitive. For samples with a pronounced surface roughness like the thin-film solar cell samples investigated in this study, PEEM is challenging since the contrast mechanisms described above can be dominated by topographical contrast, which will be discussed in conjunction with the data presented below. More detailed information on the PEEM technique[12–15] and its application to applied materials science[16–19] and thin-film solar cell structures[8,20–23] can be found in respective literature.

RESULTS AND DISCUSSION

Fig. 1 shows PEEM images of the investigated (Zn,Mg)O/CISSe sample excited with (a) a Hg discharge lamp ($h\nu = 5.1$ eV) and (b) soft x-rays ($h\nu = 177$ eV) collecting all emitted electrons. FOV for both images is 10 μm. The dark (bright) areas of the images correspond to low (high) electron emission intensity. The features at the edge and outside of the FOV are artefacts caused by the applied normalization and drift-correction procedures. Since the work functions of ZnO and MgO are very similar and both smaller than $h\nu_{Hg}$,[24] the observed large intensity variation in the Hg-PEEM image in Fig. 1(a) is not a work function related contrast but can rather mostly be ascribed to the sample topography (for scanning electron microscopy images of the bare CISSe absorber, see, e.g., Ref. 3). The X-PEEM image measured with 177 eV shown in Fig. 1(b) is essentially dominated by secondary electrons and hence this PEEM image also represents the sample topography. A comparison between Figs. 1(a) and 1(b) confirms that the Hg-PEEM image is dominated by topography features, as every feature can be related to a topography feature in the X-PEEM image. Note that the X-PEEM image (illuminated from the top right in Fig. 1(b)) exhibits shadowed regions due to the more gracing incidence geometry as compared to the Hg discharge illumination.

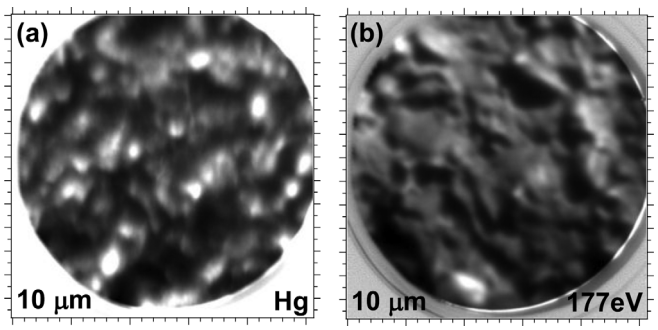

FIG. 1. PEEM image of a 1 nm (Zn,Mg)O/CISSe recorded with (a) Hg discharge lamp ($h\nu = 5.1$ eV) and (b) soft x-ray ($h\nu = 177$ eV) excitation. The field of view is 10 μm. Dark areas correspond to lower, light areas to higher electron emission intensities.

Fig. 2 shows laterally averaged XPS spectra of the (Zn,Mg)O/CISSe sample recorded with different excitation energies (using the PEEM as regular electron analyser) leading to different 1/e attenuation lengths of the electrons (i.e., probing depths). While the inelastic mean free path λ of the shallow core level electrons for the 654 eV excited data is ~1.4 nm, it is only ~0.6 nm when exciting with 142 eV.[25] Hence, while with $h\nu = 654$ eV also the absorber can be probed through the (Zn,Mg)O layer, the absorber-related photoemission peaks (Se 3d and In 4d) are significantly attenuated in the more surface sensitive 142 eV spectrum. The higher decrease of the In 4d line intensity as compared to that of the Se 3d can be explained by the changes in photoionization cross section σ for the In 4d and Se 3d photoelectrons when decreasing $h\nu$ from 654 to 142 eV; while $\sigma_{Se\ 3d}$ increases by a factor of approx. 15, $\sigma_{In\ 4d}$ only increases by a factor of approx. 1.7.[26]

The observable Na 2p photoemission line is indicative for the well-known presence of sodium in the proximity of

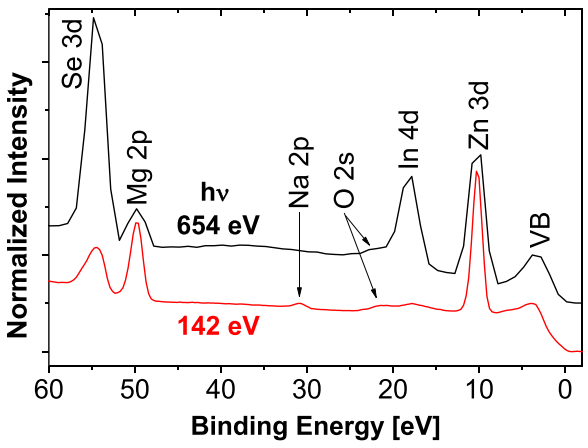

FIG. 2. Spatially integrating XPS spectra of the shallow core levels (as indicated) of a CISSe sample covered with a nominal 1 nm thick (Zn,Mg)O layer. The red spectrum was excited with 142 eV and the black spectrum with 654 eV photons, respectively.

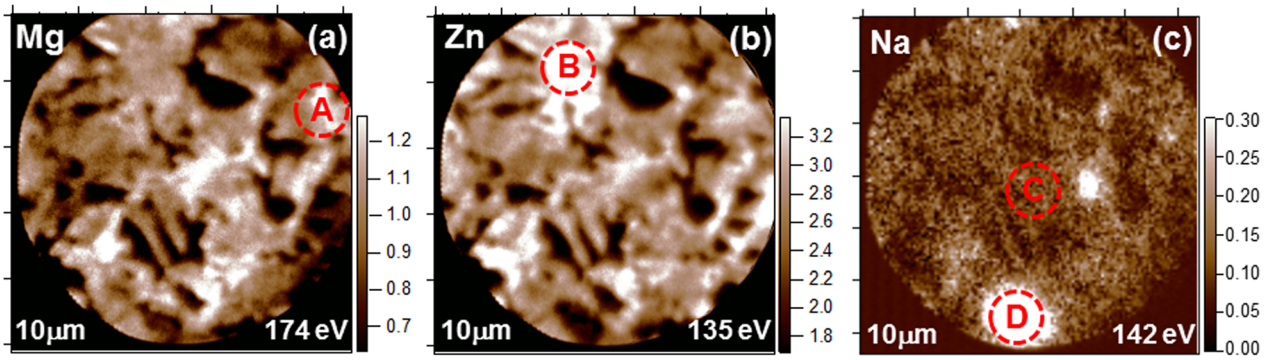

FIG. 3. X-PEEM images presenting the spatial intensity distribution of the (a) Mg 2 p, (b) Zn 3 d, and (c) Na 2 p photoemission. The field of view is 10 μm. The regions A–D of local XPS measurements (shown in Fig. 4) are indicated.

the CISSe surface.[27] Usually, Na stems from the employed soda-lime glass substrate and diffuses through the Mo back contact and the chalcopyrite thin film during absorber formation at elevated (500 °C–600 °C) temperature, accumulating at the inner (i.e., grain boundaries) and outer chalcopyrite surface.[27] In the past, several beneficial effects have been attributed to the incorporation of Na.[27] However, if the available Na amount is too high, it also can have a detrimental impact on the device performance.[27] Thus, it is important to control the amount of Na incorporated into the chalcopyrite absorber, which – for the samples studied here – is done by employing a diffusion barrier between glass substrate and molybdenum and applying a Na precursor on the Mo back contact prior CIGSSe preparation.[28] The effect and its importance of a homogeneous Na incorporation into the CIGSSe absorber w.r.t. the solar cell performance will be discussed in more detail in conjunction with our findings presented in Figs. 3(c) and 4(b) below.

For quantification of the Mg/(Zn+Mg) ratio, the Mg 2p and Zn 3d lines were fitted using Voigt profiles and linear backgrounds. Correcting the determined intensities with the respective σ-values,[26] the Mg/(Zn+Mg) ratio of the (Zn,Mg)O cover layer was computed. (Note that since the Mg 2p and Zn 3d photoemission lines are energetically close together their information depth and detector characteristics are very similar and hence no further corrections are applied.) While for the 654 eV measurement, we find the Mg/(Zn+Mg) ratio to be 0.40 ($\pm$ 0.10); for the more surface sensitive 142 eV data, the

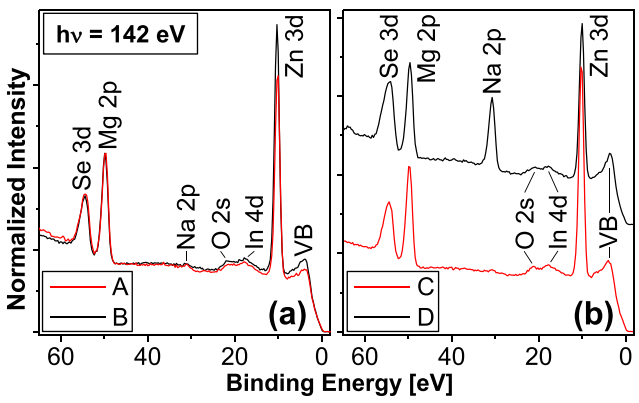

FIG. 4. Local XPS spectra (normalized to the Mg 2 p photoemission line) of (a) regions A and B and (b) regions C and D as indicated in Fig. 3.

Mg/(Zn+Mg) is 0.50 ($\pm$0.10). Both ratios are higher compared to the Mg/(Zn+Mg) = 0.30 composition of the (Zn,Mg)O sputter target, but agree very well with results of our previous XPS study.[7] The fact that the more surface sensitive measurement shows the higher Mg content confirms our previous conclusion that Zn is incorporated into the upper region of the CISSe absorber forming Zn-Se or Zn-S bonds and resulting in a (Zn,Mg)O layer which is Zn-depleted (Mg-rich) in the proximity of the interface.[7] Although single phase (Zn,Mg)O is reported for Mg contents as high as 50%—if grown on ZnO buffer layers[29]—usually the nonequilibrium solubility limit of MgO in ZnO is found to be reached for Mg/(Zn+Mg) ratios of $\geq$approx. 40%.[30,31] In consequence, the separation/segregation of MgO in the proximity of the (Zn,Mg)O/CISSe interface can also be not excluded.

To address the question whether spatially separated MgO phases are present, we used laterally resolved energy-filtered X-PEEM for the spectroscopic imaging of the (Zn,Mg)O/CISSe interface structure. Figs. 3(a)–3(c) show the Mg, Zn, and Na X-PEEM images, respectively. Element specificity is achieved by tuning the excitation energy and analyzer energy on a particular characteristic photoemission line (here: Mg 2p [hν = 174 eV], Zn 3d [hν = 135 eV], and Na 2p [hν = 142 eV]). The images in Fig. 3 are difference images calculated by subtracting background images recorded at ca. 2–5 eV lower kinetic energy than the respective photoemission line from the images recorded right on the photoemission lines. Comparing the X-PEEM image in Fig. 1(b) with Figs. 3(a)–3(c)), a similar pattern of dark areas can be observed confirming that these regions are shadowed by topography features of the (Zn,Mg)O/CISSe sample surface. However, a comparison between the Mg and Zn X-PEEM images reveals significant additional intensity variations, which cannot be attributed to the topography (i.e., areas which appear bright for the Zn X-PEEM and darker for the Mg X-PEEM and vice versa). In order to quantify the magnitude of these variation, we have also collected spatially resolved XPS spectra using hν = 142 eV, which are shown for area A (indicated in the Mg X-PEEM image, Fig. 3(a)) and area B ($\rightarrow$ Zn X-PEEM image, Fig. 3(b)). These areas show either high Mg or Zn content, respectively, and the corresponding spectra are depicted in Fig. 4(a) normalized to the Mg 2p photoemission line. It can be observed that the respective Zn 3d line intensity is significantly higher

in spectrum B. In order to quantify the respective Mg/(Zn+Mg) ratios, the photoemission lines were simultaneously fitted using Voigt profiles (with coupled Lorentzian and Gauss widths) and linear backgrounds. We determine Mg/(Zn+Mg) ratios of 0.49 (±0.10) for area A and 0.44 (±0.10) for area B. While the first value corresponds well with the average composition determined from the 142 eV data shown in Fig. 2, the Mg/(Zn+Mg) ratio in area B is (11.4 ± 0.7)% lower (than that in area A). Note the different error bars; while the absolute composition numbers contain the uncertainty of σ, the indicated relative change in composition is less error prone, as only the uncertainty in the determination of the Zn 3d and Mg 2p line intensities contribute. The fact that the Mg/(Zn+Mg) ratio in area A is in good agreement with the average Mg/(Zn+Mg) composition points to a rather complicated chemical surface/interface structure in which an area with an absolute high Mg count rate as depicted in Fig. 3(a) does not necessarily mean a high Mg/(Zn+Mg) ratio. Despite the high Mg/(Zn+Mg) composition, this could be interpreted as indication for the presence of single phase (Zn,Mg)O (as opposed to spatially separated MgO and ZnO dominated areas). However, note that a layer composed of rather homogeneously distributed ZnO and MgO nanocrystals can also not be excluded based on the here presented X-PEEM data. Taking the determined Mg/(Zn+Mg) ratios [area A: 0.49 and area B: 0.44 (±0.1)] and reported Mg/(Zn+Mg) ratio dependent band gap values of (Zn,Mg)O[32] into account, this would translate into (Zn,Mg)O band gap fluctuations of (60 ± 30) meV. Interestingly, we recently found indication for a very similar spatially band gap variation (40 meV) for high-efficiency Cu(In,Ga)Se_2 solar cell absorber surfaces caused by a variation of the Ga/(In+Ga) composition.[8] While the effects of spatially varying absorber band gaps on the performance of respective solar cell devices have previously been discussed in detail,[8,33] similar studies addressing the respective impact of electronic structure fluctuations of the emitter are scarce. However, similar to the effect of absorber band gap fluctuations, it is expected that the emitter band gap variations observed here might lead to an increase in the saturation current density and a corresponding decrease of the open circuit voltage. As the Mg/(Zn+Mg) composition of the emitter is used to deliberately tune the electronic alignment at the emitter/absorber interface,[4,5] a negative impact of the revealed surface/interface structure fluctuations on cell efficiencies can be expected.

In addition to different spatial distributions of Mg and Zn, we can also identify a significant accumulation of Na in several areas confined to approx. 2 μm (see area D in Fig. 3(c)). The respective XPS spectrum of area D is compared in Fig. 4(b) to that of area C. While a significant Na 2p signal can be identified in the XPS spectrum of area D, no major Na 2p intensity can be observed in the spectrum of area C. As already pointed out above, the presence of sodium can be beneficial for the performance of chalcopyrite-based thin-film solar cells.[27] However, this local high Na content is expected to degrade the CISSe material quality. In a standard device configuration with a CdS buffer layer deposited in a chemical bath, this accumulation of Na would not be an issue, since Na would be removed from the absorber surface during the induction period of the chemical bath deposition, in which the sample surface is essentially exposed to (i.e., etched in) aqueous ammonia.[34] In the buffer-free case studied here—in which the emitter is directly sputtered onto the chalcopyrite absorber—the revealed Na accumulation must, however, be considered in the future development of (Zn,Mg)O/CISSe based devices.

SUMMARY AND CONCLUSION

In summary, we have investigated the chemical structure of the (Zn,Mg)O/CISSe thin-film solar cell structure by spectroscopic imaging using a photoemission electron microscope. We find fluctuations in the Mg/(Zn+Mg) composition and the local accumulation of sodium in the proximity of the emitter/absorber interface. Furthermore, the comparison of spatially integrating with local XPS results suggests the presence of single-phase (Zn,Mg)O material, although the derived Mg/(Zn+Mg) ratio exceeds reported nonequilibrium solubility limits.[30,31] Based on the combination of these *spatially* resolved results and the *vertically* resolved findings reported in, e.g., Ref. 7, it is now possible to draw a more detailed picture of the complex (Zn,Mg)O/CISSe interface structure, which is a prerequisite for further knowledge-based solar cell optimization.

ACKNOWLEDGMENTS

Partial financial support by the European Commission within the ATHLET project (contract 019680) was gratefully acknowledged. Furthermore, R.G.W., R.F., D.G., and M.B. are thankful to the Helmholtz-Association (VH-NG-423) for financial support, and R.F. additionally acknowledges support by the German Academic Exchange Agency (DAAD; 331 4 04 002).

[1]M. A. Green, K. Emery, Y. Hishikawa, W. Warta, and E. D. Dunlop, Prog. Photovolt: Res. Appl. **20**, 606 (2012).
[2]P. Jackson, D. Hariskos, E. Lotter, S. Paetel, R. Wuerz, R. Menner, W. Wischmann, and M. Powalla, Prog. Photovolt: Res. Appl. **19**, 894 (2011).
[3]M. Bär, H.-J. Muffler, Ch.-H. Fischer, S. Zweigart, F. Karg, and M. C. Lux-Steiner, Prog. Photovolt: Res. Appl. **10**, 173 (2002).
[4]T. Minemoto, Y. Hashimoto, T. Satoh, T. Negami, H. Takakura, and Y. Hamakawa, J. Appl. Phys. **89**, 8327 (2001).
[5]F. Erfurth, A. Grimm, J. Palm, T. P. Niesen, F. Reinert, L. Weinhardt, and E. Umbach, Appl. Phys. Lett. **98**, 142107 (2011).
[6]Th. Glatzel, H. Steigert, R. Klenk, and M. Ch. Lux-Steiner, *Technical Digest of the 14th Photovoltaic Solar Energy Conference PVSEC* (2004), Vol. 2, pp. 707–708.
[7]F. Erfurth, B. Hußmann, A. Schöll, F. Reinert, A. Grimm, I. Lauermann, M. Bär, Th. Niesen, J. Palm, S. Visbeck, L. Weinhardt, and E. Umbach, Appl. Phys. Lett. **95**, 122104 (2009).
[8]R. G. Wilks, I. Repins, M. A. Contreras, R. Félix, J. Herrero-Albillos, L. Tati-Bismaths, F. Kronast, R. Noufi, and M. Bär, Appl. Phys. Lett. **101**, 103908 (2012).
[9]J. Palm, V. Probst, W. Stetter, R. Toelle, S. Visbeck, H. Calwer, T. Niesen, H. Vogt, O. Hernandez, M. Wendl, and F. H. Karg, Thin Solid Films **451–452**, 544 (2004).
[10]M. Bär, W. Bohne, J. Röhrich, E. Strub, S. Lindner, M. C. Lux-Steiner, Ch.-H. Fischer, T. P. Niesen, and F. Karg, J. Appl. Phys. **96**, 3857 (2004).
[11]F. Kronast, J. Schlichting, F. Radu, S. K. Mishra, T. Noll, and H. A. Dürr, Surf. Interface Anal. **42**, 1532 (2010).
[12]E. Brüche, Zeitschrift für Physik **86**, 448 (1933).
[13]E. Bauer, Rep. Prog. Phys. **57**, 895 (1994).
[14]S. Heun, Hyomen Kagaku **26**, 721 (2005).

[15]Th. Schmidt, A. Sala, H. Marchetto, E. Umbach, and H.-J. Freund, Ultramicroscopy **126**, 23–32 (2013).
[16]Y. Yamaguchi, S. Takakusagi, Y. Sakai, M. Kato, K. Asakura, and Y. Iwasawa, J. Mol. Catal. A **141**, 129 (1999).
[17]M. Kiskinova, e-J. Surf. Sci. Nanotechnol. **2**, 1 (2004).
[18]G. Xiong, R. Shao, S. J. Peppernick, A. G. Joly, K. M. Beck, W. P. Hess, M. Cai, J. Duchene, J. Y. Wang, and W. D. Wie, JOM **62**, 90 (2010).
[19]S. Pookpanratana, R. France, R. Félix, R. Wilks, L. Weinhardt, T. Hofmann, L. T. Bismaths, S. Mulcahy, F. Kronast, T. D. Moustakas, M. Bär, and C. Heske, J. Phys. D: Appl. Phys. **45**, 105401 (2012).
[20]K. Müller, I. Burkov, and D. Schmeisser, Thin Solid Films **431–432**, 307 (2003); **480–481**, 291 (2004).
[21]J. Fritsche, S. Gunst, E. Golusda *et al*., Thin Solid Films **387**, 161 (2000).
[22]K. Kanai, T. Miyazaki, T. Wakita *et al*., Adv. Funct. Mater. **20**, 2046 (2010).
[23]C. Pettenkofer, A. Hofmann, W. Bremsteller, C. Lehmann, and F. Kelleter, Ultramicroscopy **119**, 102 (2012).
[24]In J. Y. Lim, J. S. Oh, B. D. Ko, J. W. Cho, S. O. Kang, G. Cho, H. S. Uhm, and E. H. Choi, J. Appl. Phys. **94**, 764 (2003), depending on orientation the work function of MgO single crystals is reported to be 4.22–5.07 eV; in K. Ellmer, A. Klein, and B. Rech, *Transparent Conductive Zinc Oxide: Basics and Applications in Thin Film Solar Cells* (Springer, Berlin, 2008), p. 143 depending on the $O_2/(Ar+O_2)$ ratio during deposition the work function of polycrystalline ZnO layers is reported to be 4.1–5.1 eV.
[25]S. Tougaard, QUASES-IMP-TPP2M code for the calculation of the inelastic electron mean free path, Version 2.2 (http://www.quases.com/)—based on S. Tanuma, C. J. Powell, and D. R. Penn, Surf. Interface Anal. **21**, 165 (1993).
[26]J. J. Yeh and I. Lindau, Atomic Data and Nuclear Data Tables **32**, 1 (1985).
[27]For a recent summary of the "sodium effect" please refer to X. Song, R. Caballero, R. Félix, D. Gerlach, C. A. Kaufmann, H.-W. Schock, R. G. Wilks, and M. Bär, J. Appl. Phys. **111**, 034903 (2012), references therein.
[28]J. Palm, V. Probst, and F. H. Karg, Sol. Energy **77**, 757 (2004).
[29]T. Takagi, H. Tanaka, S. Fujita, and S. Fujita, Jpn. J. Appl. Phys., Part 2 **42**, L401 (2003).
[30]A. Ohtomo, M. Kawasaki, T. Koida, K. Masubuchi, H. Koinuma, Y. Sakurai, Y. Yoshida, T. Yasuda, and Y. Segawa, Appl. Phys. Lett. **72**, 2466 (1998).
[31]S. Sadofev, S. Blumstengel, J. Cui, J. Puls, S. Rogaschewski, P. Schäfer, Yu. G. Sadofyev, and F. Henneberger, Appl. Phys. Lett. **87**, 091903 (2005).
[32]In order to estimate the impact of the Mg/(Zn+Mg) fluctuations on the (Zn,Mg)O band gap (E_g), we fitted the $z = Mg/(Zn+Mg)$ dependent band gap values reported in Refs. 30 and 31 with a polynomial 2nd order in the given $0 \le z \le 0.45$ range: $E_g(z)\ [eV] = 3.31 + 3.11 \times z - 2.13 \times z^2$. Assuming that the computed $E_g(z)$ relation is also valid for higher Mg contents resulting in single-phase (Zn,Mg)O, the observed differences in the local XPS derived Mg/(Zn+Mg) compositions have been translated into a band gap variation.
[33]U. Rau and J. H. Werner, Appl. Phys. Lett. **84**, 3735 (2004); J. H. Werner, J. Mattheis, and U. Rau, Thin Solid Films **480–481**, 399 (2005); S. Siebentritt, Sol. Energy Mater. Sol. Cells **95**, 1471 (2011).
[34]L. Weinhardt, Th. Gleim, O. Fuchs, C. Heske, E. Umbach, M. Bär, H.-J. Muffler, Ch.-H. Fischer, M. Ch. Lux-Steiner, Y. Zubavichus, T. P. Niesen, and F. Karg, Appl. Phys. Lett. **82**, 571 (2003).